VIP Stimuli-Responsive Materials Very Important Paper

DOI: 10.1002/ange.201408010

Breathing Pores on Command: Redox-Responsive Spongy Membranes from Poly(ferrocenylsilane)s**

*Kaihuan Zhang, Xueling Feng, Xiaofeng Sui, Mark A. Hempenius, and G. Julius Vancso**

Abstract: *Redox-responsive porous membranes can be readily formed by electrostatic complexation between redox active poly(ferrocenylsilane) PFS-based poly(ionic liquid)s and organic acids. Redox-induced changes on this membrane demonstrated reversible switching between more open and more closed porous structures. By taking advantage of the structure changes in the oxidized and reduced states, the porous membrane exhibits reversible permeability control and shows great potential in gated filtration, catalysis, and controlled release.*

Porous polymeric membranes play a pivotal role in membrane science and technology as they raise many opportunities for fundamental research and enable a wide range of applications in many fields of practical relevance.[1] In this regard, porous polyelectrolyte membranes are particularly appealing and versatile for a variety of applications such as separation, controlled release, catalysis, biointerfacing, and sensing, because of the tunable electrostatic charge and high physical and chemical stability.[2] Stimuli-responsive materials, which exhibit large and sharp changes in response to small variations of external parameters such as temperature, pH, ionic strength, electromagnetic fields, and changes in the redox state, are attracting increasing interest.[3] Functional porous polyelectrolyte membranes can be prepared to demonstrate stimuli-responsive characteristics capable of reversibly changing the pore size or switching between open and closed porous structure after exposure to stimulation. For example, Rubner et al. assembled nanoporous anti-reflection coatings from phase-separated polyelectrolyte multilayer films of poly(allylamine hydrochloride)/poly(acrylic acid) that undergo a reversible pH-induced swelling transition.[4] Minko et al. reported a pH-responsive thin film from cross-linked poly(2-vinylpyridine) and 1,4-diiodobutane with two-dimensionally arranged submicron pores. The cross-linked membranes demonstrated pH-dependent swelling, which had a strong influence on the pore size.[2a,5]

Poly(ionic liquid)s (PIL), a subclass of polyelectrolytes featuring an ionic liquid species in each monomer repeating unit synthesized by direct polymerization or post-polymerization modification, have emerged as promising materials for a variety of applications.[6] Recently, Yuan et al. and other researchers reported on a series of polyelectrolyte complexes and membranes made from imidazolium-based poly(ionic liquid)s that showed utilization potential as catalyst support,[7] in dye adsorption,[8] in pH sensing,[9a] and in stimulus actuation.[9b] Incorporation of redox active polymers in such membrane frameworks can provide unique responsive platforms. Poly(ferrocenylsilane) (PFS), which is composed of alternating ferrocene and silane units in the main chain, exhibits redox-responsive behavior inheriting from the high density of redox centers.[10] PFS-based PIL bearing imidazolium moieties have already demonstrated practical potential in nanogels, hydrogels,[11] molecular release,[12] and electrochemical sensing.[13] Herein we introduce a template-free route to porous membranes from PFS-based PIL and poly(acrylic acid). Coating this porous membrane onto the surface of an electrode or other substrates yields platforms with a high interface-to-volume area that is due to to the porosity of the membrane, and a switchable surface with redox-responsiveness that is due to the redox activity of the constituting macromolecules.

Figure 1a illustrates the structure of a cationic polyelectrolyte composed of a poly(ferrocenylsilane) main chain and vinylimidazolium bis(trifluoromethylsulfonyl)imide side groups (PFS-VImTf_2N) and a common organic acid poly(-acrylic acid) (PAA), which were employed as a polyelectrolyte pair to prepare the porous membrane. The synthetic route to vinylimidazolium functionalized PFS is described in detail elsewhere.[11] The counterion in the PIL was exchanged to more hydrophobic Tf_2N^- to increase hydrophobicity of this PFS-based PIL, which makes it insoluble in water but soluble in dimethylformamide (DMF). Figure 1b illustrates the fabrication procedure leading to the porous membranes. Electrostatic complexation between polycation and polyanion, generated by treatment with base, results in the formation of a porous structure.[9a] First, PFS-VImTf_2N and PAA ($M_w = 1800$) were fully dissolved in DMF at an equivalent molar ratio based on monomer units. The homogeneous solution was then cast (or spin-coated) onto a silicon (or gold) substrate and dried at 80 °C for 30 min. During evaporation, mainly DMF escaped from the membrane surface, leading to a concentrated and homogeneous polymer blend (partial vapor pressure of DMF 9 kPa at 80 °C, 0.5 kPa at 25 °C). After drying, the film was immersed in a 0.5 wt %

[*] K. Zhang, X. Feng, Dr. X. Sui, Dr. M. A. Hempenius, Prof. G. J. Vancso
Materials Science and Technology of Polymers and MESA+Institute for Nanotechnology, University of Twente
P.O. Box 217, 7500 AE Enschede (The Netherlands)
E-mail: G.J.Vancso@utwente.nl

[**] This work was financially supported by the MESA+ Institute for Nanotechnology of the University of Twente and by the Netherlands Organization for Scientific Research (NWO, TOP Grant 700.56.322, Macromolecular Nanotechnology with Stimulus Responsive Polymers; NWO 728.011.205, ChemThem: Out-of-equilibrium self-assembly).

Supporting information for this article is available on the WWW under http://dx.doi.org/10.1002/anie.201408010.

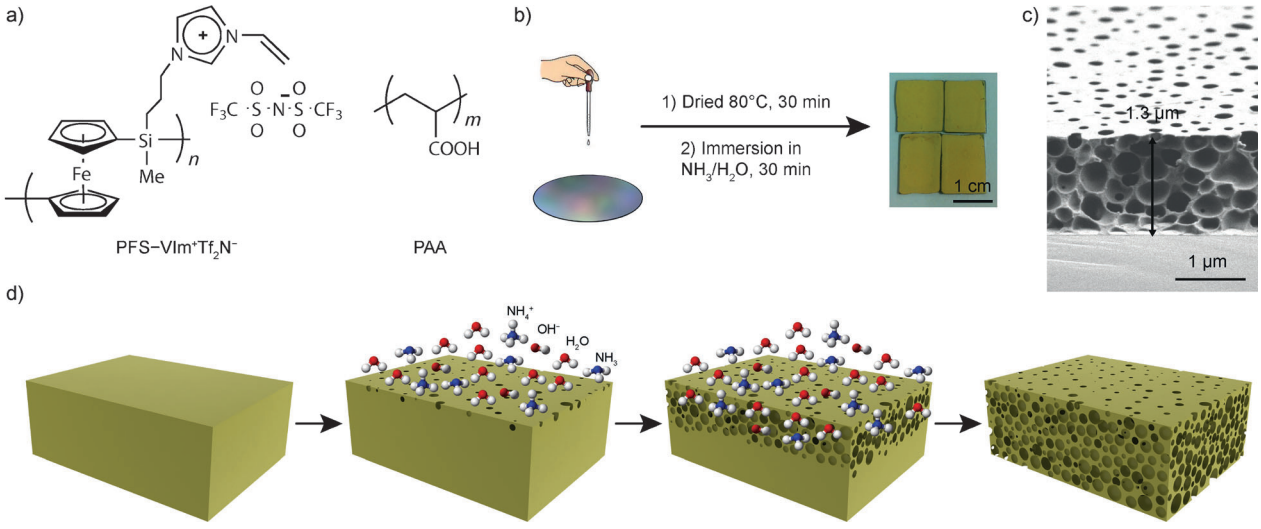

Figure 1. Preparation of the porous membrane. a) Chemical structures of PFS-VImTf$_2$N and PAA used in this study. b) Illustration of the preparation of a porous membrane from a polymer blend solution of PFS-VImTf$_2$N and PAA in DMF. c) SEM images of a representative porous membrane obtained with a thickness of 1.3 µm. d) Representation illustrating the pore-formation process induced by ammonia diffusion.

aqueous NH_3 solution (pH 11.2, 20 °C). This process led to charging of the acrylic acid moieties, restructuring of the polymeric film on nanoscale, and finally the formation of a stable sub-microporous structure. An amber-colored membrane (Figure 1 b, color related to PFS) with different thickness values (0.5 to 20 µm; Supporting Information, Figure S2) was readily obtained by variation of volume and concentration of the polymer blend.

Interestingly, a three-dimensionally interconnected porous structure with pore sizes of 250 ± 70 nm formed during the immersion step. From cross-sectional SEM images, the porosity of the bulk membrane was estimated to be 65 %. The complex membranes have openings on their surface and interconnections underneath with neighboring cells. No significant differences in pore size were found between different areas across the membrane (Supporting Information, Figure S3). In control experiments, membranes could not be obtained from the pristine PFS-VImTf$_2$N polymer solution (Supporting Information, Figure S4a) and only few pores were formed by soaking the PFS-VImTf$_2$N/PAA physical blend in neutral water without NH_3 (Figure S4b). Under insufficient treatment time by aqueous NH_3 solution the porous structure could not be fully developed and a bilayer membrane consisting of a porous sponge layer with a dense polymer blend underneath was observed in this case (Figure S4c). This clearly indicates the pore formation is controlled by diffusion of aqueous NH_3 solution into layers away from the free surface.

Aqueous NH_3 solution as a weak base initiates pore formation by deprotonating carboxylic acid (COOH) groups of the PAA chains to form carboxylate groups (COO^-), thus activating interchain ionic bonding and structural rearrangements between PAA and surrounding cationic PFS-VImTf$_2$N. We note that PAA has a relatively low dissociation constant 3.2×10^{-7} (reported value for the solution pKa of PAA is 6.5[14]) and thus essentially no porous structure can be formed under neutral conditions (Supporting Information, Figure S4b). At pH over 10, most of the COOH groups were transformed into the COO^- form. Ionization of PAA and the poor water solubility of PFS-VImTf$_2$N play an important role in the process of pore formation. A molecular mechanism responsible for pore formation for similar structures has been recently proposed.[9b] Pore formation was attributed to phase separation of a PIL in contact with water that contributes to the formation of the pore walls, while the simultaneous electrostatic complexation between the PIL and a carboxylic acid-bearing C-pillar[5]arene finally gave the ionic network, stabilizing the pore structures.[9b] In view of structural similarities, we propose a similar mechanism to take place also in our system. FTIR spectra confirmed the deprotonation of COOH groups after immersion in the aqueous NH_3 solution (Supporting Information, Figure S5).

The electrochemical properties of the porous membranes were investigated by cyclic voltammetry (CV). Figure 2 shows representative CV results in 0.1 M aqueous $NaClO_4$ versus an Ag/AgCl electrode. Electrochemical oxidation of the porous membrane was accompanied by a color change from amber to green-blue and the membrane turned back to amber upon reduction (Figure 2 a).[15] The double-wave voltammogram (Figure 2 a) as described previously, indicates electron overlap by Si bridges between the neighboring redox active ferrocene units along the PFS chains.[16] The influence of the scan rate on the current is depicted in the Supporting Information, Figure S6. At lower scan rates, linear dependencies between peak current and scan rate were found which are characteristic for surface-confined electroactive species. At higher scan rates, peak currents are linearly proportional to the square root of scan rate, which indicates a diffusion controlled process. The porous membrane shows stable electrochemical performance during 15 cycles of scanning.

Scanning electron microscopy (SEM) images (Figure 2 b, c) show variations of the size of the cellular structures when comparing membranes in the oxidized and reduced state. In the oxidized form, the membranes had a visibly

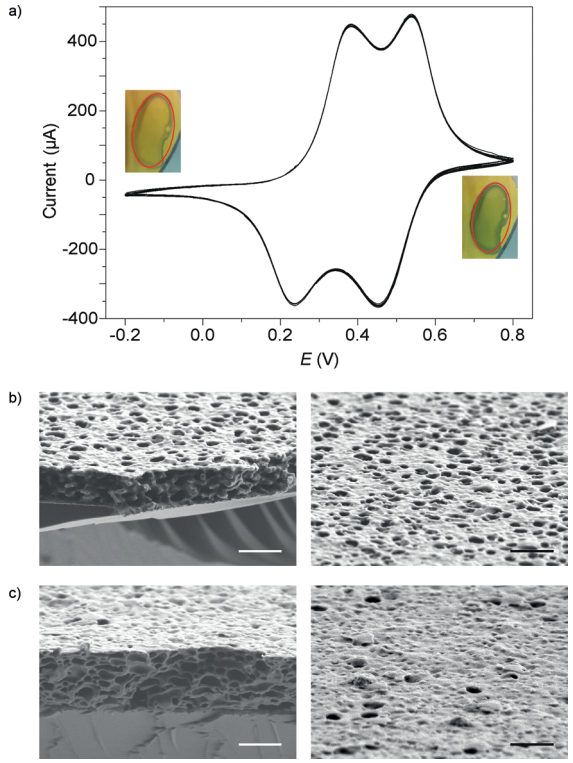

Figure 2. Electrochemical characterization of porous membranes and surface switching. a) Cyclic voltammograms of PFS-VImTf$_2$N/PAA complex membrane on Au substrate at a scan rate of 5 mVs^{-1} (15 full cycles). b), c) Cross-sectional and surface SEM images of porous membranes after oxidation at 0.6 V for 10 min (b), and then reduction at −0.2 V for 10 min (c). Scale bar: 1 μm.

higher density of the openings. Cross-sectional SEM images also show significant differences between the porous structures before and after oxidation. The porous membranes have a higher density of closed cells in the reduced state as compared to the oxidized state. The redox responsive variation of the cellular morphology originates from the oxidation of the ferrocenyl groups of PFS.

The excess positive charge along the PFS main chain increases ionic interactions between PFS and the surrounding PAA, which results in redistribution of polymer chains in the pore walls and enlarges the interconnecting window size between adjacent pores, leading to a more open structure (Supporting Information, Figure S7). This responsive behavior will be further studied by in situ small-angle X-ray scattering (SAXS).

PFS chains have been shown to reduce silver ions to the elemental metal by oxidation of the ferrocenyl groups. In the case of cylindrical PFS micelles[17] or PFS microparticles,[12] this redox reaction led to the formation of silver nanoparticles in the micellar core as well as at the surface of microgel particles. Here, when the porous membrane was immersed in a 10 mM $AgNO_3$ aqueous solution, a color change from light yellow to grey was observed. Silver nanoparticles (26 ± 4 nm) were formed on the surface of the membrane (Figure 3; Supporting Information, Figure S8).

The switching process between open and closed porous states can be also triggered reversibly via chemical oxidation

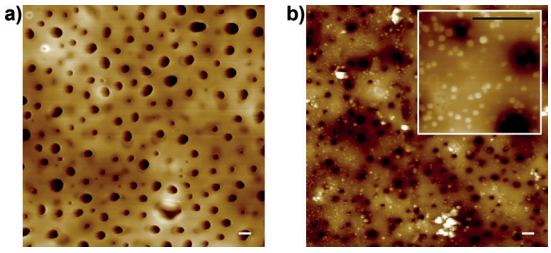

Figure 3. AFM topography image of a pristine PFS-VImTf$_2$N/PAA complex membrane (a) and after immersion in a 10 mM $AgNO_3$ aqueous solution for 10 min (b). Scale bars: 200 nm.

and reduction. This was documented by a treatment using 10 mM $Fe(ClO_4)_3$ and 10 mM ascorbic acid aqueous solution, respectively (Figure 4). Compared to electrochemical oxidation and reduction, chemical treatment allowed us to change the redox state in one minute owing to high diffusion rates in the porous membrane. The porous membrane in oxidized and reduced states, stimulated by chemical redox agents, showed similar structures to those that were triggered by electrochemical stimuli.

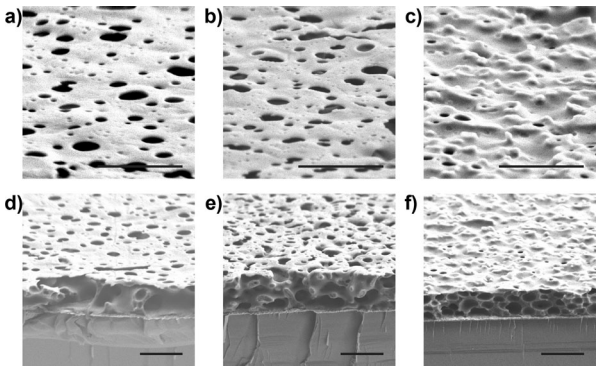

Figure 4. Surface and cross-sectional SEM images of PFS-VImTf$_2$N/PAA complex membrane: untreated membrane (a and d), after oxidation by 10 mM $Fe(ClO_4)_3$ aqueous solution (b and e), and then following reduction by 10 mM ascorbic acid in aqueous solution (c and f). Scale bar: 1 μm.

As shown in one of our earlier studies, polyelectrolyte multilayer capsules, composed of polyanions and polycations of PFS, show fast expansion accompanied by a drastic permeability increase in response to a redox trigger.[15] Here, reversible control of the membrane structure between more open or more closed cell structures after exposure to chemical redox agents allowed us to switch the permeability of the membrane. The permeability of the porous films was studied by measuring permeate flux of milli-Q water (pH 7) under static pressure. The PFS-VImTf$_2$N/PAA complex membrane was first deposited on a cellulose membrane (Whatman cellulose filter paper, Grade 589/3, pore size: 2 μm, thickness: 160 μm) and then fixed to a filter holder connected to a water column (50 cm, 5 kPa pressure, pH 7). The flux of pure water was determined by recording the time used for 10 mL water to be filtered through the given membrane geometry. The membrane was oxidized and

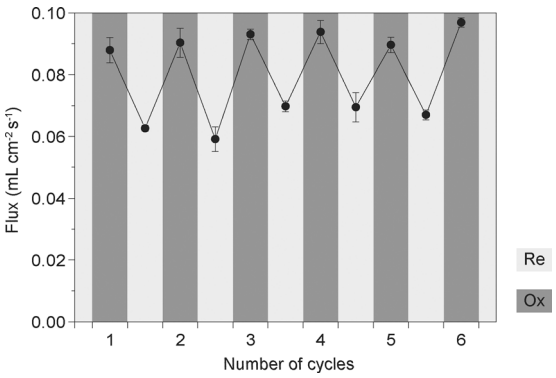

Figure 5. Repeated reversible switching of the flow of pure water under 5 kPa pressure for the oxidized and reduced porous membranes.

reduced by 10 mM $Fe(ClO_4)_3$ and ascorbic acid for several repeated cycles. The average flow rate was $0.092 \pm 0.004\ mL\,cm^{-2}\,s^{-1}$ in the oxidized state and $0.064 \pm 0.005\ mL\,cm^{-2}\,s^{-1}$ in the reduced states, respectively (Figure 5). The permeability switching originates from the changes in interconnectivity between pores, induced by oxidization and reduction of PFS. In the reduced state, the pores are less interconnected, as is evident from a zoomed-in SEM image (Supporting Information, Figure S7), which shows small windows in the pore walls. Upon oxidation, interconnectivity between pores within the membrane increases (Figure 4e,f). The increased interconnectivity between pores directly influences cutoff characteristics of the membrane, as is evident from the higher permeability in the oxidized state.

Finally we note that recently, Elbert et al. demonstrated redox-controlled gating for a hybrid membrane constructed from a mesoporous silica template and chemically grafted side-chain ferrocene-containing polymers.[18] Porosity in this case was provided by the inert substrate, and not by structural rearrangements of the responsive polymer matrix itself.

In summary, we report a template-free method to prepare redox-responsive porous polyelectrolyte membranes from PFS-based poly(ionic liquid)s and poly(acrylic acid). The PFS-VImTf_2N/PAA complex membrane demonstrated redox responsive behavior, which had a strong influence on porous structure and enabled switching of permeability. The membranes we described have application potential in various areas, including selective filtration, enzyme-entrapped membranes for bio-sensing, controlled loading and release, catalysis in microfluidic reactors, and sensing.

Experimental Section

Preparation of PFS-VImTf_2N: Poly(ferrocenyl(3-iodopropyl)methylsilane) ($M_w = 3.21 \times 10^5\ g\,mol^{-1}$, $M_n = 1.67 \times 10^5\ g\,mol^{-1}$, $M_w/M_n = 1.9$) was prepared according to established procedures.[19] Imidazolium functionalized PFS was obtained by allowing poly(ferrocenyl(3-iodopropyl)methylsilane) to react with 1-vinylimidazole in THF/DMSO at 60 °C for 24 h. The iodide counterions were first exchanged with chloride counterions by dialysis in 0.1M aqueous NaCl and subsequently exchanged with Tf_2N^- conterions by precipitation in aqueous LiTf_2N solution.

Instruments and characterization: Molar mass values were determined by gel permeation chromatography in THF using a polystyrene calibration curve. ^{1}H NMR spectra were recorded by employing a Bruker Avance III 400 MHz spectrometer. FTIR spectra were obtained by a Bruker Vertex 70v spectrometer. SEM was carried out using a HR-LEO 1550 FEF SEM instrument at 1 kV. A Dimension D3100 (Digital Instruments, Veeco-Bruker, Santa Barbara, CA) AFM was operated in the tapping mode to obtain the surface morphology of the membrane. Electrochemistry measurements were carried out on gold-coated silicon substrates in aqueous $NaClO_4$ (0.1M) using an Autolab PGSTAT 10 electrochemical workstation. Cyclic voltammograms were recorded between −0.2 and 0.8 V using a Ag/AgCl reference electrode and a Pt counter electrode.

Received: August 7, 2014
Published online: October 24, 2014

Keywords: electrochemistry · poly(ferrocenylsilane)s · porous membranes · redox trigger · stimuli-responsive materials

[1] a) D. Wu, F. Xu, B. Sun, R. Fu, H. He, K. Matyjaszewski, *Chem. Rev.* **2012**, *112*, 3959 – 4015; b) D. L. Gin, R. D. Noble, *Science* **2011**, *332*, 674 – 676; c) K. V. Peinemann, V. Abetz, P. F. Simon, *Nat. Mater.* **2007**, *6*, 992 – 996.
[2] a) I. Tokarev, M. Orlov, S. Minko, *Adv. Mater.* **2006**, *18*, 2458 – 2460; b) X. Hu, J. Huang, W. Zhang, M. Li, C. Tao, G. Li, *Adv. Mater.* **2008**, *20*, 4074 – 4078.
[3] a) M. A. C. Stuart, W. T. S. Huck, J. Genzer, M. Müller, C. Ober, M. Stamm, G. B. Sukhorukov, I. Szleifer, V. V. Tsukruk, M. Urban, F. Winnik, S. Zauscher, I. Luzinov, S. Minko, *Nat. Mater.* **2010**, *9*, 101 – 113; b) C. de Las Heras Alarcón, S. Pennadama, C. Alexander, *Chem. Soc. Rev.* **2005**, *34*, 276 – 285; c) X. Sui, X. Feng, M. A. Hempenius, G. J. Vancso, *J. Mater. Chem. B* **2013**, *1*, 1658 – 1672; d) J. Ge, Y. Yin, *Angew. Chem. Int. Ed.* **2011**, *50*, 1492 – 1522; *Angew. Chem.* **2011**, *123*, 1530 – 1561.
[4] J. A. Hiller, J. D. Mendelsohn, M. F. Rubner, *Nat. Mater.* **2002**, *1*, 59 – 63.
[5] M. Orlov, I. Tokarev, A. Scholl, A. Doran, S. Minko, *Macromolecules* **2007**, *40*, 2086 – 2091.
[6] T. Ueki, M. Watanabe, *Macromolecules* **2008**, *41*, 3739 – 3749.
[7] a) Q. Zhao, P. Zhang, M. Antonietti, J. Yuan, *J. Am. Chem. Soc.* **2012**, *134*, 11852 – 11855; b) Y. Xiong, J. Liu, Y. Wang, H. Wang, R. Wang, *Angew. Chem. Int. Ed.* **2012**, *51*, 9114 – 9118; *Angew. Chem.* **2012**, *124*, 9248 – 9252; c) P. Zhang, J. Yuan, T. P. Fellinger, M. Antonietti, H. Li, Y. Wang, *Angew. Chem. Int. Ed.* **2013**, *52*, 6028 – 6032; *Angew. Chem.* **2013**, *125*, 6144 – 6148.
[8] Q. Zhao, S. Soll, M. Antonietti, J. Yuan, *Polym. Chem.* **2013**, *4*, 2432 – 2435.
[9] a) Q. Zhao, M. Yin, A. P. Zhang, S. Prescher, M. Antonietti, J. Yuan, *J. Am. Chem. Soc.* **2013**, *135*, 5549 – 5552; b) Q. Zhao, J. W. C. Dunlop, X. Qiu, F. Huang, Z. Zhang, J. Heyda, J. Dzubiella, M. Antonietti, J. Yuan, *Nat. Commun.* **2014**, *5*, 4293.
[10] a) I. Manners, *Chem. Commun.* **1999**, *10*, 857 – 865; b) V. Bellas, M. Rehahn, *Angew. Chem. Int. Ed.* **2007**, *46*, 5082 – 5104; *Angew. Chem.* **2007**, *119*, 5174 – 5197; c) G. R. Whittell, M. D. Hager, U. S. Schubert, I. Manners, *Nat. Mater.* **2011**, *10*, 176 – 188.
[11] X. Sui, M. A. Hempenius, G. J. Vancso, *J. Am. Chem. Soc.* **2012**, *134*, 4023 – 4025.
[12] X. Sui, L. Shui, J. Cui, Y. Xie, J. Song, A. van den Berg, M. Hempenius, G. J. Vancso, *Chem. Commun.* **2014**, *50*, 3058 – 3060.
[13] X. Feng, X. Sui, M. A. Hempenius, G. J. Vancso, *J. Am. Chem. Soc.* **2014**, *136*, 7865 – 7868.
[14] J. Choi, M. F. Rubner, *Macromolecules* **2005**, *38*, 116 – 124.
[15] Y. J. Ma, W. F. Dong, M. A. Hempenius, H. Mohwald, G. J. Vancso, *Nat. Mater.* **2006**, *5*, 724 – 729.

[16] a) R. Rulkens, A. J. Lough, I. Manners, S. R. Lovelace, C. Grant, W. E. Geiger, *J. Am. Chem. Soc.* **1996**, *118*, 12683 – 12695; b) M. Péter, R. G. H. Lammertink, M. A. Hempenius, G. J. Vancso, *Langmuir* **2005**, *21*, 5115 – 5123.
[17] a) X. S. Wang, H. Wang, N. Coombs, M. A. Winnik, I. Manners, *J. Am. Chem. Soc.* **2005**, *127*, 8924 – 8925; b) H. Wang, X. S. Wang, M. A. Winnik, I. Manners, *J. Am. Chem. Soc.* **2008**, *130*, 12921 – 12930.
[18] J. Elbert, F. Krohm, C. Rüttiger, S. Kienle, H. Didzoleit, B. N. Balzer, T. Hugel, B. Stühn, M. Gallei, A. Brunsen, *Adv. Funct. Mater.* **2014**, *24*, 1591 – 1601.
[19] M. A. Hempenius, F. F. Brito, G. J. Vancso, *Macromolecules* **2003**, *36*, 6683 – 6688.

